Electric-field tuning of the Bragg peak in large-pore TiO_2 inverse shell opals

E. Graugnard, J. S. King, S. Jain, and C. J. Summers*
School of Materials Science & Engineering, Georgia Institute of Technology, Atlanta, Georgia 30332, USA

Y. Zhang-Williams and I. C. Khoo†
Department of Electrical Engineering, Pennsylvania State University, University Park, Pennsylvania 16802, USA
(Received 13 September 2005; revised manuscript received 25 October 2005; published 13 December 2005)

Inverse opals with large connection pores were fabricated by infiltrating sintered polystyrene opal templates using low-temperature atomic layer deposition of TiO_2 and subsequently dissolving the polystyrene in toluene. The dielectric lattice, consisting of overlapping air spheres in a TiO_2 matrix, was then infiltrated with nematic liquid crystal, with some samples having received a prior hydrophobic surface treatment. The specular reflectance is shown to depend not only on electric-field amplitude, but also on film structure. In the hydrophobic-treated sample, a 20 nm shift of the Bragg peak was observed for an applied electric field of 50 kV/cm.

DOI: 10.1103/PhysRevB.72.233105 PACS number(s): 42.70.Qs, 42.70.Df

The two most commonly studied three-dimensional photonic crystal (3DPC) structures include the opal and inverse opal, each of which possesses a pseudo- (or directional) photonic band gap in the (111) direction that forbids propagation of radiation within the crystal for a certain range of frequencies.[1] Experimentally the presence of the pseudogap is observed as a strong reflectance peak, or Bragg peak, whose wavelength λ_{Bragg} is determined by both the periodicity of the dielectric modulation and the effective refractive index n_{eff} of the material. At normal incidence λ_{Bragg} is given by

$$\lambda_{Bragg} = 2d_{111}n_{eff} \tag{1}$$

where d_{111} is the spacing between (111) planes. Following the initial work of Busch *et al.* and Yoshino *et al.*,[2,3] several groups have focused on using liquid crystals (LCs) to tune λ_{Bragg} by controlling n_{eff}, which for an opal infiltrated with liquid crystal is given by

$$n_{eff} = \sqrt{f_{opal}n_{opal}^2 + f_{LC}n_{LC}^2} \tag{2}$$

where f_{opal} and f_{LC} are the volume fractions of the opal and liquid crystal, respectively. Since LCs possess a dielectric anisotropy Δn_{LC}, the refractive index n_{LC} may be tuned between the ordinary (n_o) and extraordinary (n_e) index values by controlling the orientation of the molecules.[4] From Eq. (2), we note that the largest Δn_{LC}, weighted by the largest f_{LC}, produces the largest Δn_{eff} and therefore the largest Bragg peak tuning by Eq. (1).

In an opal, the volume available for liquid crystal infiltration consists of octahedral and tetrahedral voids between the spheres of the fcc structure. Kang *et al.* studied the degree of liquid crystal alignment that would be expected for such constrained volumes for either parallel or homeotropic (normal to surface) alignment of the LC on the surface of the opal spheres. However, for either surface alignment, the small LC volume of only 26% greatly limits the effect of any orientational tuning. Nonetheless, several groups have observed Bragg peak tuning to varying degrees, with either temperature or applied electric field.[3,5–8] On the other hand, inverted opal structures, consisting of a network of interconnected spherical air cavities in a dielectric backbone, provide a LC volume fraction of 74%. Both the volume increase and the change in cavity geometry lead to a larger possible Δn_{eff} and thus increased Bragg peak tunability.[9–15] For example, Mach *et al.* studied the response of liquid crystals confined to connected and disconnected spherical cavities,[9] and Kubo *et al.* recently reported electric-field tuning of SiO_2 and polymer inverse opals using photoinduced phase transitions.[15] While large electric-field-induced tunability has been reported for a polymer inverse opal,[11] a significant degree of tunability has yet to be reported for a high-dielectric inverse opal using an applied electric field. The latter case is more desirable for many 3DPC applications because of its higher dielectric contrast and larger Bragg peak width.

In this paper, we report successful electrical Bragg peak tuning in high-dielectric large-pore inverse opals. To form this structure, which consists of *overlapping* air spheres in a high dielectric backbone, we fabricated large-pore TiO_2 inverse shell opals, with air cavity filling fractions of $\sim$0.81, which were subsequently infiltrated with the nematic liquid crystal 5CB (EMD Chemicals Inc., $\Delta n_{LC} \simeq 0.18$). For an applied electric field of 50 kV/cm (5 V/μm), we observed dynamic tuning of the Bragg peak wavelength by 14 nm in a hydrophilic sample and by 20 nm in a sample with a hydrophobic surface treatment. Hysteresis of the Bragg peak position was observed for the hydrophobic treated sample while no hysteresis was observed for the nontreated sample. Analysis of the Bragg peak position indicates that complete liquid crystal alignment was obtained at an applied field of $\sim$50 kV/cm.

Opal templates, 10 μm in thickness, were fabricated by forced self-assembly of monodisperse polystyrene spheres (329 nm diameter, Duke Scientific) within a confinement cell.[16] To reduce the opal template air void volume, the samples were sintered for 1 h at 100 °C,[17] which increased the diameter of the sphere contact points, as illustrated in Fig. 1(a). After sintering, the templates were infiltrated with amorphous TiO_2 (refractive index=2.31 at 800 nm) using atomic layer deposition (ALD) by the method we reported previously,[18] but with the temperature lowered to 80 °C and

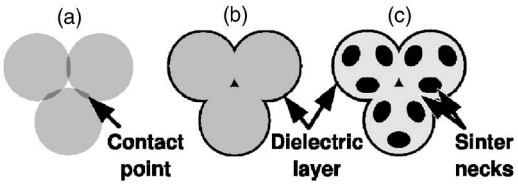

FIG. 1. Schematic steps for fabricating a large-pore inverse shell opal. (a) An opal template is sintered to increase the diameter of the contact points. (b) The sintered template is infiltrated with a high-dielectric material. (c) The template spheres are removed to create a lattice of overlapping air spheres in a dielectric backbone.

the cycle times extended to allow for complete diffusion through the constricted pores of the sintered template. This technique allowed for facile infiltration of opal templates as it is a surface-limited growth technique that uses cyclic, sequential precursor exposure to deposit film coatings one layer per cycle.[18–20] Using a conformal deposition technique, such as ALD, the maximum filling level is 86% of the pore volume (or 22.4% of the total volume) for an unsintered template, but is reduced slightly in a sintered template by the deformation of the lattice.[18] The fully infiltrated samples were next ion milled to remove the top half of the outermost layer of infiltrated spheres, which provided access to the interconnected polystyrene lattice. A schematic of the fully infiltrated and ion-milled template is shown in Fig. 1(c). The samples were immersed in toluene overnight to completely remove the polystyrene template, forming a large-pore inverse opal, as illustrated schematically in Fig. 1(d) and shown experimentally in the scanning electron microscope (SEM) images of Fig. 2. Compared to both opals and normal inverse opals, this open large-pore structure provided a much less constricting volume for LC reorientation under applied fields, which facilitated the largest possible Δn_{LC}.

To study the effect of liquid crystal surface pinning in the inverse opal cavities, a portion of the sample was treated to produce a hydrophobic surface. The sample was immersed in water-saturated hexanes, and a drop of fluorinated chlorosilane[21] was introduced to the hexanes and allowed to diffuse into the inverse opal, forming a fluorinated coating on the cavity surfaces. This treatment is similar to commonly used techniques to control the degree of liquid crystal pinning.[6] The resulting surface of the treated sample was hydrophobic, whereas the surface of the untreated sample was hydrophilic.

Next, individual grains of the inverse opals were selected and deposited on indium tin oxide–(ITO)-coated aluminosilicate substrates and then covered with ITO top plates to create cells. Spacers made from 10-μm-thick SU-8 photoresist were used to control the separation between ITO surfaces. The hydrophilic sample was infiltrated with liquid crystal using capillary forces with both sample and LC at $\sim$50 °C. The hydrophobic sample could not be infiltrated by the direct application of LC to the sample cell. Instead, the LC was dissolved in ethanol at $\sim$5% by volume, and the LC-ethanol mixture was repeatedly applied to the sample cell, which was heated to $\sim$50 °C between applications to evaporate the ethanol, leaving the LC deposited within the film.

Specular reflectance measurements were acquired at each stage of sample fabrication in order to follow the development of the Bragg peak. The spectra for the hydrophobic sample are shown in Fig. 3 and were used to quantify the filling fractions of both the TiO_2 backbone and the infiltrated LC using Eqs. (1) and (2), modified for the additional materials. The Bragg peak of the initial opal template was ob-

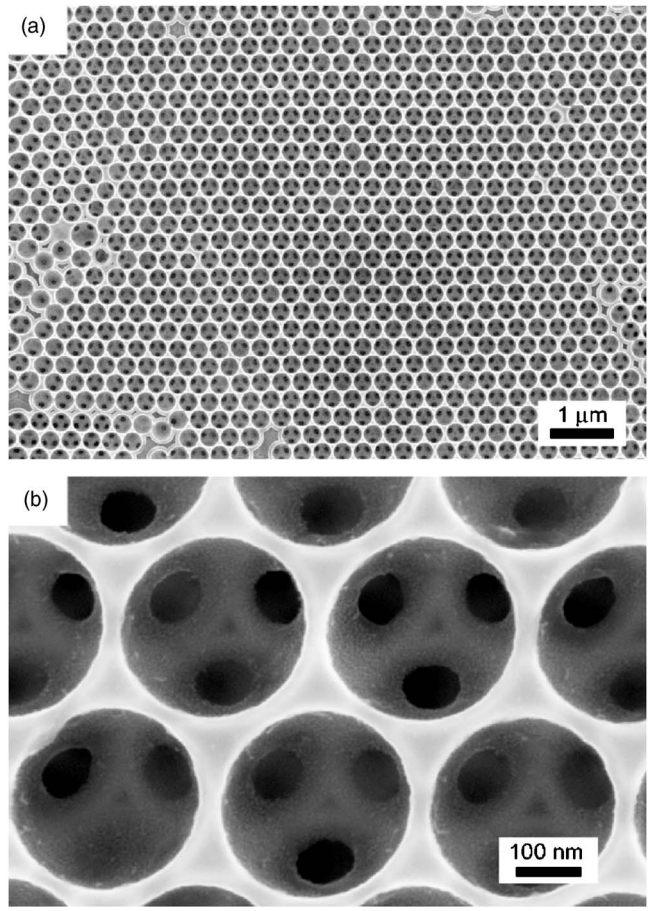

FIG. 2. SEM images of a large-pore inverse shell opal at low (a) and high (b) magnifications. The diameters of the contact points between the spheres were significantly larger than those in a typical inverse opal.

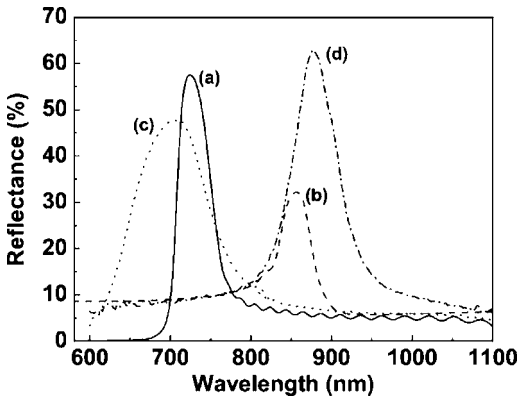

FIG. 3. Reflectance at each stage of fabrication. (a) Initial opal template, (b) sintered and infiltrated opal, (c) large-pore inverse opal, and (d) liquid-crystal-infiltrated large-pore inverse opal.

served at 726 nm (measured at 15° with respect to normal incidence). This peak shifted to 855 nm after sintering and TiO_2 infiltration. Full TiO_2 infiltration was confirmed when additional TiO_2 ALD cycles failed to shift the peak further, resulting in a final TiO_2 filling fraction of 0.168, leaving over ~81% of the volume available for LC infiltration. Upon inversion, the Bragg peak shifted to 704 nm, which was below the position of the initial Bragg peak of the opal template, and broadened due to the increase in the dielectric contrast. Infiltration with LC shifted the Bragg peak to 876 nm. Similar to the infiltration of TiO_2, the full infiltration of LC was confirmed when repeated application of the LC failed to produce a further shift of the Bragg peak. For these samples, 100% LC infiltration refers to complete infiltration of the spherical cavities. The air pockets at the center of the opal interstitials remain sealed by the TiO_2 backbone. The hydrophilic sample was completely infiltrated with LC upon the first application to the cell, while the hydrophobic sample required several LC-ethanol applications to obtain the same peak shift. The spectra of the LC-infiltrated samples were acquired at normal incidence using a microscope to study the single grains individually.

Based on the analysis of the Bragg peak position during each stage of sample fabrication, it was possible to calculate the average refractive index of the infiltrated LC. For 100% infiltration, we found $n_{LC}^{expt}=1.583$. Since the LC was infiltrated above its nematic-isotropic phase transition temperature (~32 °C), the initial molecular orientation was random, but for reflectance measurements made at room temperature, the LC was in the nematic phase within each cavity of the inverse opal film. However, the director field changes from cavity to cavity resulting in an average isotropic orientation over the entire sample grain.[9,14] Thus, based on the refractive indices for 5CB, $n_o=1.522$ and $n_e=1.706$, the average LC refractive index is expected to be 1.586, which agrees very well with the measured value.

Dynamic tunability of the LC-infiltrated samples was observed by measuring the reflectance spectra as a function of applied bias using square wave modulation at 1 kHz. Figures 4(a) and 4(b) show the spectra for the hydrophilic and hydrophobic samples, respectively, and Fig. 5 plots the peak positions versus applied field. The hydrophilic sample exhibited a maximum shift of 14 nm toward the uv for an applied amplitude of 50 V and returned to the exact position when the bias was removed. The hydrophobic sample, however, exhibited a maximum peak shift of 18 nm for a bias of 50 V, but the peak did not return to the initial wavelength when the bias was removed and displayed a slight hysteresis. It is interesting to note that when the modulation frequency of the applied bias was increased to 25 kHz, the Bragg peak shifted an additional 2 nm for the hydrophobic sample, producing an overall shift of 20 nm. No additional shift was observed for the hydrophilic sample. For a shift of 20 nm, the Bragg peak position was 856 nm, which according to Eq. (2) gives $n_{LC}^{ave}=1.52$, which agrees with the ordinary index for 5CB. This indicates that the molecules were completely aligned along the electric-field lines. From Fig. 5, it is observed that there was no threshold voltage required to tune the Bragg peak, which saturated for an applied field of ~30 kV/cm for the hydrophilic sample and ~40 kV/cm for the hydrophobic sample. For each sample the peak width increased on average by ~1%.

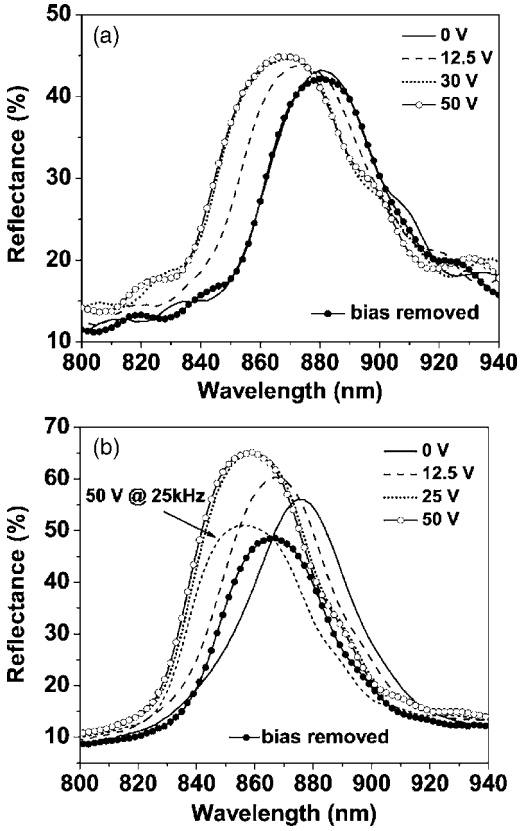

FIG. 4. Reflectance spectra for several applied biases for both the hydrophilic (a) and hydrophobic (b) samples. Thin film interference fringes are observed imposed on the Bragg peak in the spectra in (a).

The presence of the hysteresis observed for the hydrophobic sample (and its absence in the hydrophilic sample) can be understood in terms of the surface pinning of the LC molecules. In the hydrophilic sample, the LC molecules were strongly pinned to the TiO_2 surface. Thus, when the applied

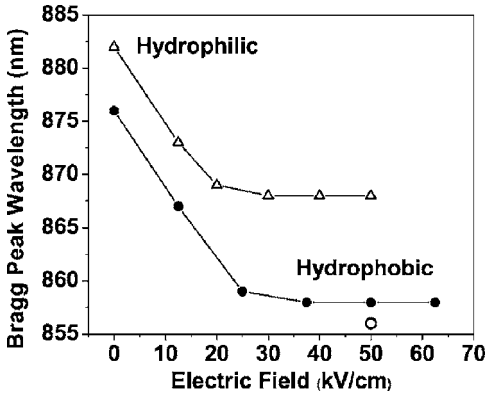

FIG. 5. Bragg peak position versus applied electric field at 1 kHz for the hydrophilic (open triangles) and hydrophobic (filled circles) samples. The open circle is the peak position for the hydrophobic sample with 50 V applied at 25 kHz.

bias was removed, strong restoring forces reoriented the LC molecules within the cavities. This pinning effect may also explain why the Bragg peak did not shift as far into the uv. For the hydrophobic sample, the LC molecules were not pinned as strongly to the cavity surface, due to the chlorosilane treatment, and thus exhibited hysteresis when the bias was removed because of much weaker restoring torques. Furthermore, the large pores connecting the spherical cavities promote director alignment within the sample grain, which would also enhance the hysteresis effect in the absense of strong restoring forces.

In conclusion, we reported successful electrical Bragg peak tuning of liquid crystal infiltrated large-pore TiO_2 inverse shell opals. Tuning was observed in both untreated hydrophilic samples and samples treated with a hydrophobic surface coating. A Bragg peak shift of 20 nm, observed for the hydrophobic sample, indicated complete field-induced alignment of the LC molecules. Additionally, the width of the Bragg peak was observed to increase with applied electric field. The significant Bragg peak tuning reported here provides the important next step in fabricating tunable three-dimensional photonic crystals. We are currently working to increase the air filling fraction of the large-pore inverse opal structure and are investigating materials with larger electro-optic coefficients for faster and wider Bragg peak tunability.

This work was supported by the U.S. Army Research Office under MURI Contract No. DAAD19-01-1-0603. Y.W. is supported by PSU-NSF-MRSEC Center for Nanoscale Science under Grant No. DMR-0213623.

*Electronic address: chris.summers@mse.gatech.edu
†Electronic address: ick1@psu.edu

[1] H. Míguez, C. López, F. Meseguer, A. Blanco, L. Vázquez, R. Mayoral, M. Ocaña, V. Fornés, and A. Mifsud, Appl. Phys. Lett. **71**, 1148 (1997).
[2] K. Busch and S. John, Phys. Rev. Lett. **83**, 967 (1999).
[3] K. Yoshino, Y. Shimoda, Y. Kawagishi, K. Nakayama, and M. Ozaki, Appl. Phys. Lett. **75**, 932 (1999).
[4] I.-C. Khoo, *Liquid Crystals: Physical Properties and Nonlinear Optical Phenomena* (Wiley & Sons, New York, 1995).
[5] K. Yoshino, S. Satoh, Y. Shimoda, H. Hajii, T. Tamura, Y. Kawagishi, T. Matsui, R. Hidayat, A. Fujii, and M. Ozaki, Synth. Met. **121**, 1459 (2001).
[6] D. Kang, J. E. Maclennan, N. A. Clark, A. A. Zakhidov, and R. H. Baughman, Phys. Rev. Lett. **86**, 4052 (2001).
[7] Q.-B. Meng, J. Appl. Phys. **89**, 5794 (2001).
[8] Y. Shimoda, M. Ozaki, and K. Yoshino, Appl. Phys. Lett. **79**, 3627 (2001).
[9] P. Mach, P. Wiltzius, M. Megens, D. A. Weitz, K.-H. Lin, T. C. Lubensky, and A. G. Yodh, Phys. Rev. E **65**, 031720 (2002).
[10] G. Mertens, Appl. Phys. Lett. **80**, 1885 (2002).
[11] M. Ozaki, Y. Shimoda, M. Kasano, and K. Yoshino, Adv. Mater. (Weinheim, Ger.) **14**, 514 (2002).
[12] S. Kubo, Z.-Z. Gu, K. Takahashi, Y. Ohko, O. Sato, and A. Fujishima, J. Am. Chem. Soc. **124**, 10950 (2002).
[13] S. Gottardo, D. S. Wiersma, and W. L. Vos, Physica B **338**, 143 (2003).
[14] S. Kubo, Z.-Z. Gu, K. Takahashi, A. Fujishima, H. Segawa, and O. Sato, J. Am. Chem. Soc. **126**, 8314 (2004).
[15] S. Kubo, Z.-Z. Gu, K. Takahashi, A. Fujishima, H. Segawa, and O. Sato, Chem. Mater. **17**, 2298 (2005).
[16] S. H. Park, D. Qin, and Y. Xia, Adv. Mater. (Weinheim, Ger.) **10**, 1028 (1998).
[17] B. Li, J. Zhou, L. Li, and Z. Gui, J. Mater. Sci. **40**, 2611 (2005).
[18] J. S. King, E. Graugnard, and C. J. Summers, Adv. Mater. (Weinheim, Ger.) **17**, 1010 (2005).
[19] J. S. King, C. W. Neff, C. J. Summers, W. Park, S. Blomquist, E. Forsythe, and D. Morton, Appl. Phys. Lett. **83**, 2566 (2003).
[20] A. Rugge, J. S. Becker, R. G. Gordon, and S. H. Tolbert, Nano Lett. **3**, 1293 (2003).
[21] (Tridecafluoro-1,1,2,2-Tetrahydrooctyl)-1-trichlorosilane, United Chemical Technologies, Inc.